Probing Solvation and Reaction Coordinates of Ultrafast Photoinduced Electron-Transfer Reactions Using Nonlinear Spectroscopies: Rhodamine 6G in Electron-Donating Solvents[†]

Qing-Hua Xu, Gregory D. Scholes, Mino Yang, and Graham R. Fleming*

Department of Chemistry, University of California, Berkeley, and Physical Biosciences Division, Lawrence Berkeley National Laboratory, Berkeley, California 94720-1460

Received: June 7, 1999; In Final Form: September 8, 1999

The reaction kinetics as well as the solvation dynamics of the photoinduced electron-transfer (ET) reaction from the electron-donating solvents dimethylaniline (DMA) and diethylaniline (DEA) to rhodamine 6G (R6G) are elucidated using complementary information from transient grating (TG) and three-pulse photon echo peak shift (3PEPS) measurements. The data are contrasted with those obtained from TG and 3PEPS studies in the "unreactive" solvents ethanol and dimethyl sulfoxide. New methods are employed to model these data using nonlinear response functions expressed in terms of both solvation dynamics and reaction kinetics. A three-level model, including a component in the response function to account for excited-state absorption, is used to model the 3PEPS and TG data. It is also demonstrated that 3PEPS retrieves information concerning the reaction coordinate as well as solvation information. We conclude that for R6G/DMA, rapid photoinduced ET occurs on a time scale of $\tau_a \sim 85$ fs and for the R6G/DEA system $\tau_a \sim 160$ fs. An excited-state absorption contribution to the signals that we associate with back-electron transfer was observed with time constants τ_b = 4.0 ps for R6G/DMA (15% contribution) and τ_b = 6.9 ps for R6G/DEA (20% contribution). Subsequently, the cooling and relaxation (i.e. ground-state recovery) occurs on a time scale of τ_c = 19 ps (R6G/DMA) and τ_c = 50 ps (R6G/DEA). We attribute the τ_c to solvent-limited reequilibration on the ground-state free energy curve.

I. Introduction

Electron-transfer (ET) reactions have attracted considerable attention as model, fundamental chemical reactions due to their universality in chemistry and biology.[1−16] ET rates are influenced strongly by the redox properties of donor and acceptor molecules, as well as the dielectric properties of the solvent. In some regimes, the solvation time scales are also important.[17−19] In the present work we investigate the interplay between these effects in a system where the electron donor is also the solvent bath. Use of standard time-resolved techniques such as pump−probe or spontaneous fluorescence decay does not always allow for a complete description of ultrafast electron-transfer processes. Fluorescence only provides information on the initially excited state, whereas disentanglement of the reaction kinetics from solvation dynamics and vibrational cooling is not always straighforward in pump−probe spectroscopy. In this paper we explore the use of photon echo and transient grating spectroscopies to elucidate the dynamics of ultrafast electron transfer in solution. By utilizing and extending the methodology of Yang et al.,[20] we show that forward- and back-electron-transfer rates, as well as solvation dynamics, can be extracted from such data.

Solvation dynamics plays a crucial role in many chemical and physical processes in the condensed phase.[16−25] Recently, there has been substantial progress in understanding chemical dynamics in liquid systems.[21−23] In particular, the effect of solvation on the rate of electron transfer has been under intensive study.[17−19,24−26] Solvation can influence an ET reaction in two ways. It can act in a static sense to change the energy of reactants
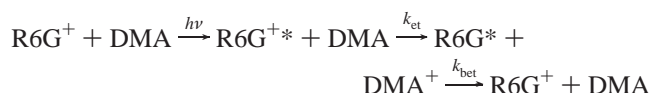
and products compared with their energy in the gas phase (i.e. it affects their redox properties). It can also act in a dynamic way by exchanging energy and momentum with the reactants to provide the impetus necessary to overcome the reaction barrier and then enable the products to dissipate excess energy. In the present work, we investigate a rapid ET reaction from solvent to solute which is affected by the fastest time scales of solvation (e.g. the ultrafast inertial response)[27,28] and we investigate the subsequent evolution of the products. We have probed both the reaction kinetics and the solvation dynamics using two ultrafast nonlinear spectroscopies: three-pulse photon echo peak shift (3PEPS) and transient grating (TG). Both techniques contain similar information, but the 3PEPS measurement emphasizes the solvation dynamics (i.e. fluctuations in the electronic energy gap caused by coupling to the solvent bath), while the TG experiment emphasizes population dynamics. In combination, these methods allow us to resolve much of the dynamical information underpinning the ET reaction.

In recent years photoinduced intermolecular electron transfer between various dyes in electron-donating solvents (such as aniline and dimethylaniline) have been widely studied.[6−9,29] The electron donor (the solvent) and acceptor (the dye molecule) are in direct contact, so no diffusional motion is needed to bring the reactants together. Thus, for certain donor−acceptor pairs the electron transfer can occur extremely rapidly after photoexcitation—for example, Zinth et al.[8] have reported the rate of ET in the oxazine/dimethylaniline system to be as fast as 80 fs. Similar observations have been reported for related systems.[6,30−33] In the present paper we report our studies of the ET reactions involving rhodamine 6G (R6G) in electron-donating solvents: *N,N*-dimethylaniline (DMA) and *N,N*-diethylaniline (DEA). We refer in these solvents as "reactive solvents". We also report

---

[†] This paper is dedicated to Kent Wilson, who has inspired, illuminated, and enriched our scientific lives.

Ultrafast Photoinduced ET Reactions

J. Phys. Chem. A, Vol. 103, No. 49, 1999 **10349**

studies of R6G in the "unreactive solvents" dimethyl sulfoxide (DMSO) and ethanol.

In reactive solvents, the following reaction occurs:

$$\text{R6G}^+ + \text{DMA} \xrightarrow{h\nu} \text{R6G}^{+*} + \text{DMA} \xrightarrow{k_{et}} \text{R6G}^* +$$
$$\text{DMA}^+ \xrightarrow{k_{bet}} \text{R6G}^+ + \text{DMA}$$

where k_{et} is the rate of photoinduced ET from DMA to R6G (which we wrote above explicitly as its natural cationic state), and k_{bet} is the back-electron-transfer rate. It has been established that the ET in these electron-donating solvent systems is approximately barrierless and proceeds much faster than the time scales of diffusive solvation.[6–9,29] By examining both the ET (population) dynamics and the solvation dynamics in detail, we aim to elucidate a picture of the reaction kinetics as well as their entanglement with solvation dynamics.

The 3PEPS and TG data we report here contain a lot of kinetic information in addition to the contributions from dephasing and solvation processes. This is particularly evident in the TG profiles, which exhibit a marked contribution from a component with negative amplitude, much like the unusual transient absorption signals reported for some isomerization reactions.[34,35] We show here that it is possible to model these data successfully using a simple three-level description. The third level denotes an S_n state that is involved in an $S_n \leftarrow S_1$ transient absorption contribution to the signal that we find to be significant from both the reactant and product states. In the analysis reported in the present work, the model takes the general and simple form of kinetically coupled three-level systems. The contributions to the third-order nonlinear response functions from excited-state absorption provide us with a significantly greater range of dynamic information than we would otherwise obtain with a one-color measurement. This is because the transient absorption from the product state contributes to the signal for much longer times than the stimulated emission (this latter transition is shifted out of resonance with the laser spectrum by the ET reaction). We use a double-sided Feynman diagram analysis to derive nonlinear response functions describing the three different contributions to our signals: ground-state recovery, stimulated emission, and excited-state absorption. We thus resolve reaction kinetics as well as solvation dynamics.

II. Experimental Section

The experimental apparatus and method of 3PEPS and TG have been described in detail previously.[36] A mode-locked titanium:sapphire oscillator (Coherent Mira) was used to seed a regenerative amplifier (Coherent RegA), the resulting 50 fs full width at half-maximum (fwhm), 800 nm output was then used to pump an OPA (Coherent 9050). Nearly transform limited pulses of 40 fs fwhm at a repetition rate of 250 kHz were produced. A center wavelength of 540 nm was used for R6G/DMA, R6G/DEA, and R6G/DMSO, while 531 nm was used for R6G/ethanol. The laser output was split into three rectilinear beams with parallel polarizations and approximately equal power. These were aligned in an equilateral triangle with each side being ca. 10 mm to enable simultaneous detection of two equally phase matched integrated three-pulse photon echo signals. All three beams were focused by a 20 cm focal length fused silica singlet lens into the sample, which was circulated through a 0.1 mm quartz flow cell. A pulse energy of 5 nJ/beam before the sample was used for the data reported here. The experiments were also performed with energies from 3 to 15 nJ, and no differences in the form of the echo signal or the peak shift were observed.
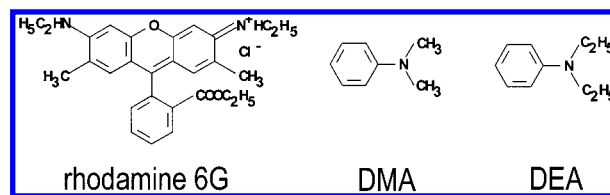

Figure 1. Structures of the electron donors and acceptor. Rhodamine 6G (R6G) is the electron acceptor; DMA and DEA are the donors.
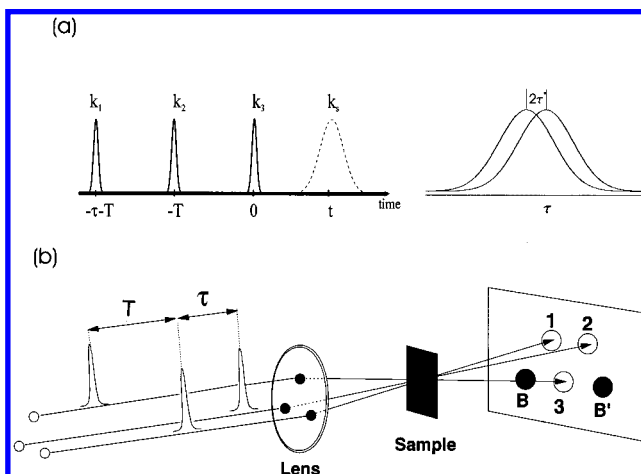

Figure 2. (a) Pulse sequence and schematic of the peak shift experiment. Three consecutive pulses with wave vectors of k_1, k_2, and k_3 are separated by τ and T. The echo field generated by the rephasing process along the phase-matched direction $k_3 + k_2 - k_1$ is pictorially shown by the dotted line. In the experiment, τ is scanned from negative to positive. The right one shows that the peak shift is half of the peak difference of the two signals (B and B′). (b) Experimental beam geometry and the two phase-matching directions $k_3 + k_2 - k_1$ (B) and $k_3 + k_1 - k_2$ (B′) for the signals.

The molecular structures of the dye molecule and solvents used in the present work are shown in Figure 1. The laser dye rhodamine 6G was purchased from Exciton Co. and was used without further purification. Spectrophotometric grade (or the otherwise highest purity) ethanol, DMSO, DMA (*N,N′*-dimethylaniline), and DEA (*N,N′*-diethylaniline) were obtained from Aldrich Chemical Co. and used as received. Absorption spectra were measured using a Shimadzu UV−visible spectrophotometer. Fluorescence spectra were measured with a Datamax Std. Fluorolog-3 fluorimeter. The rhodamine 6G solutions were made to an optical density of approximately 0.07 (in 0.1 mm path length) at the absorption maximum. The concentration was estimated to be around $<10^{-4}$ M, thus avoiding interchromophore interaction effects. To assist solvation of rhodamine 6G in DMA and DEA, a small amount of methanol (less than 1%) was added. Absorption measurements showed that such addition of methanol caused no change in the absorption shape and width.

The photon echo and transient grating signals were detected in the phase matching directions $-k_1 + k_2 + k_3$ and $k_1 - k_2 + k_3$ (Figure 2). For each population time T of the 3PEPS experiment, we scan the first coherence period τ from negative to positive time delay while measuring the time-integrated echo in the two signal directions. For the transient grating, we set τ equal to zero and scan T (signals from the two channels were averaged). All the experiments were conducted at ambient temperature (293 K).

III. Theoretical Background

III. A. Nonlinear Response Function. The line broadening and nonlinear response are determined by fluctuations of the

electronic energy gap, $\hbar\omega_{eg}$, caused by coupling to the solvent bath.[23,37-40] This introduces a time dependence of ω_{eg} for molecule i,

$$\omega_{eq}^i(t) = \langle\omega_{eg}\rangle + \epsilon_i + \delta\omega_{eg}(t) \tag{1}$$

where $\langle\omega_{eg}\rangle$ is the average value of the transition frequency and ϵ_i is a static offset from the average value $\langle\omega_{eg}\rangle$ for chromophore i, which vanishes in the case of fluid solution. $\delta\omega_{eg}(t)$ gives the dynamic contribution to the spectrum which can be described by the transition frequency correlation function, $M(t)$,

$$M(t) = \langle\delta\omega_{eg}(0)\,\delta\omega_{eg}(t)\rangle/\langle\delta\omega^2_{eg}\rangle \tag{2}$$

The associated line broadening function is given by

$$g(t) = \langle\Delta\rangle^2 \int_0^t dt_1 \int_0^{t_1} dt_2\, M'(t_2) - i\lambda \int_0^t dt_1[1 - M''(t_1)] \tag{3}$$

where the site inhomogeneity on a time scale determined by the dynamic range of the experiment is assumed to be negligible, as is the case in a liquid solvent, and $M(t) = M'(t) = M''(t)$ in the high-temperature limit.[37]

In the 3PEPS and TG measurement the integrated signals along two phase-matched directions are detected. The peak shift is half of the difference between the signal maxima (see Figure 2). The decay of the 3PEPS has been shown to follow $M(t)$ directly when the population time is longer than the solvation correlation time.[39] In the impulsive limit the integrated photon echo signal is given by

$$S(T,\tau) = \int_0^{\infty} dt\, |R(t,T,\tau)|^2 \tag{4}$$

where $R(t,T,\tau)$ is the sum of the contributions from the different pathways and depends on the dynamical systems under study, as will be discussed in detail in the following section.

III.B. Three-Level Model. There are three distinct kinetic contributions to the signals reported here: stimulated emission, SE, excited-state absorption, ESA, and ground-state recovery, GSR. If only small-amplitude nuclear motions are involved in the reaction, the time scales for the SE, ESA, and GSR would be identical. This is probably the rule rather than the exception and has been observed in many pump–probe studies of ET reactions.[41] However, if large-amplitude nuclear motion is associated with the reaction, as in twisted intramolecular charge-transfer (TICT) behavior or isomerization reactions,[42-44] SE, ESA, and GSR measure different regions along the reaction coordinate. Hence, the observed time scales differ.[45,46] For finite bandwidth laser pulses, these time scales are also very sensitive to the changes in the energy gaps associated with the corresponding transitions between states as a function of reaction coordinate.

The kinetically coupled three-level system which constitutes the three-level model is shown in Figure 3a. Following the initial excitation, the 3PEPS and TG signals arise from a population grating formed between the ground- (G) and excited E-state (E) population densities. The population initially in the reactant region e of the levels labeled E undergoes electron transfer (k_{et}) to form a charge-separated product state e′. Back-electron transfer eventually returns this product population to the ground electronic levels (G). If ESA to upper electronic state(s) F overlaps spectrally with the probe wavelength, then it will also contribute to the observed signal.

We assume that along the reaction coordinate of the E level the optical properties of the system may vary. For example, on
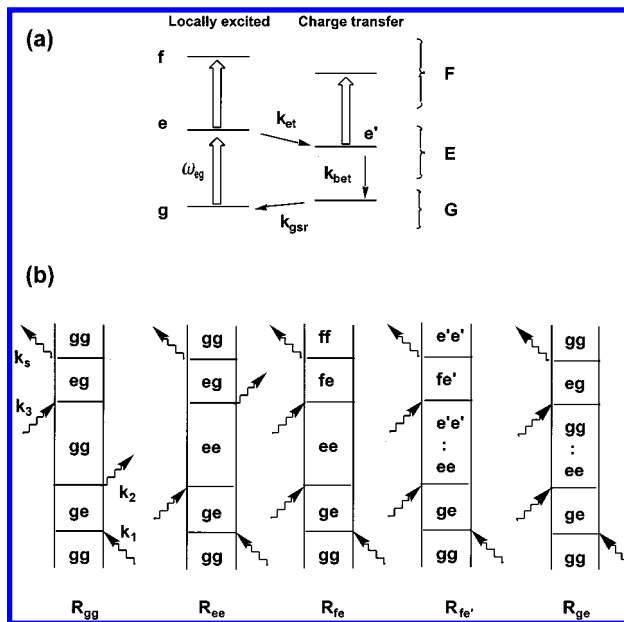

Figure 3. Three-level model (a) and the corresponding double-sided Feynman diagrams (b). G is the ground state; E is the adiabatic curve of the excited state and charge-separated state; F is the higher excited state. k_{et}, k_{bet}, and k_{gsr} denote the rate of electron transfer, back-electron transfer, and ground-state recovery, respectively.

the reactant region denoted by the e in Figure 3a, both of the G–E and E–F transitions are possible for a transient time following the initial excitation. However, as the ET reaction proceeds, the e-state population moves along the reaction coordinate to the charge-separated product state e′, and if we assume the ground-state potential is steep along the reaction coordinate, this migration of the population blocks the stimulated emission (SE) occurring between the E and G levels. If the shape of the free energy surface E resembles that of F, then an ESA contribution to the signal could persist after population of the e′ state. The region of the E level where the ESA is allowed but the SE is blocked as a result of the reaction is denoted by e′. The transition from the e state to the e′ state is regarded approximately as the electron-transfer process.

Upon relaxation of e′ (if such a process occurs), or making a transition to high vibrational states on the G surface via internal conversion, the system evolves into a "dark" state which cannot be probed by the laser due to a loss of resonance between ω_{eg} and the spectroscopic transitions. We refer to the state as dark simply because it cannot be probed with our laser spectrum— we do not imply that it does not absorb at all. Actually, for the experimental observations made in the present work, we cannot conclude if a dark state exists on the far product side of the E surface or if it only corresponds to a vibrationally hot state on the G surface. It is known that the system in the dark state eventually returns to the bottom of the G surface, upon which the optical activity is restored (ground-state recovery, GSR).

The third-order nonlinear optical response of the system should be described properly by incorporating the kinetics of transitions between the optically distinct states discussed above. For the purpose of simplicity, in this section we only discuss the optical response associated with the signal for the phase-matched direction $k_3 + k_2 - k_1$, and we assume a pulse duration that is impulsively short. Note that we do not make these assumptions in the numerical simulations reported in section IV. In our model reactive system there are five types of third-order processes, the representative Feynman diagrams, which are shown in Figure 3b. In addition to R_{gg} (ground-state

bleaching) and R_{ee} (stimulated emission), which are characteristic of the normal two-level system, we have three new contributions. Two of them—R_{fe} and $R_{fe'}$—are associated with the ESA processes from the e and e′ states, respectively. The last response function R_{ge} is associated with the ground-state recovery through the reaction cycle (e → e′ → possible dark state → g). The total response function is then given by

$$R = R_{gg} + R_{ee} - R_{fe} - R_{fe'} - R_{ge} \qquad (5)$$

The negative sign of the last three terms arises from the odd number of interactions with the ket and bra side of the double-sided Feynman diagrams. Since the ET reaction does not occur in the ground state, R_{gg} is taken to be the same as in a normal two-level system and contains only contributions from solvation dynamics (i.e. $R_{gg} = R_{gg}^0$). Hereafter, the superscript 0 denotes that a separation between solvation dynamics and kinetics has been made.

Since the ET reaction transfers the population from the e state to the e′ state, the other pathways associated with the population on the E surface should be properly scaled according to the respective population kinetics. For simplicity, Markovian population kinetics are assumed in the present work. We obtain the response function responsible for SE on the e state as

$$R_{ee} \approx R_{ee}^0 \exp(-T/\tau_a) \qquad (6)$$

where τ_a is the time scale of the e → e′ transition (lifetime of the e state), which could be assigned as the ET time. The contribution of the ESA on the e state should also decay with the lifetime of the e state τ_a:

$$R_{fe} \approx R_{fe}^0 \exp(-T/\tau_a) \qquad (7)$$

To describe the depletion of the ESA on the e′ state, we introduce another time scale τ_b which is associated with the transition from the e′ to the dark state (i.e. involving k_{bet}, cf. Figure 3). Considering the input and output of the e′ state population, we obtain

$$R_{fe'} \approx R_{fe'}^0 \frac{\tau_a^{-1}}{\tau_a^{-1} - \tau_b^{-1}}[e^{-T/\tau_b} - e^{-T/\tau_a}] \qquad (8)$$

The time scale τ_b may also contain information on the dynamics of spectral diffusion on the product side of the E surface. The response functions $R_{fe'}^0$ and R_{fe}^0 will have rephasing capability if the fluctuations of the g−e transition energy gap ω_{eg} are correlated to those of the e′(e)−f transition energy gaps $\omega_{fe'}$ (ω_{fe}); in which case the third-order process associated with the ESA will give echo signals. If the fluctuations are uncorrelated with each other, then free induction decay (FID) will be generated by the ET. If we assume that $\tau_a \ll \tau_b$ (we believe this to be the case for the present system), the sum of the two response functions associated with the ESA becomes

$$R_{fe} + R_{fe'} = R_{fe'}^0 \, e^{-T/\tau_b} + (R_{fe}^0 - R_{fe'}^0)e^{-T/\tau_a}$$

$$\approx R_{fe'}^0 \, e^{-T/\tau_b} \qquad (9)$$

which means that τ_b is indicative of the time scale for which ESA persists on the E surface. We suggest that this is mostly representative of the time scale for back-electron transfer.

We can separate out a scaling factor α from $R_{fe'}^0$ to account for the difference in the magnitude of transition moment between ground-state absorption (GSA) and ESA: $R_{fe'}^0 \approx \alpha \hat{R}_{fe'}^0$. To do

this, the Franck−Condon approximation (the separation of electronic and nuclear wave functions) is invoked, and the electronic transition moment depends only weakly on coordinate, Q: $\mu_{FE}(Q) \approx \mu_{FE}(Q_0)\langle \chi_F | \chi_E \rangle$, where χ_F and χ_E are the nuclear wave functions for the F and E states. We expect this approximation to have limited validity since such a separation is inappropriate for large-amplitude motion on a reaction coordinate connecting reactants and products. First, the electronic transition moment must depend on (reaction) coordinate: $\mu_{FE}(Q) \neq \mu_{FE}(Q_0)$. This is clear if we consider the reaction to be adiabatic and that the pure locally excited (LE) state has a different transition moment magnitude (μ_{LE}) than the pure charge-transfer (CT) state (μ_{CT}). At all coordinates, the electronic wave function can be written as a linear combination of LE and CT configurations: $\Psi_e = c_1\Psi_{LE} + c_2\Psi_{CT}$. For the reactants, $c_1 \gg c_2$, whereas the product state has $c_1 \ll c_2$. Hence, $\mu_{FE}(Q)$ changes smoothly from μ_{LE} to μ_{CT} along the reaction coordinate. Second, we do not know whether the upper excited state F is a single electronic state or a manifold of electronic states which are resonant with the laser spectrum. We cannot realistically address these issues quantitatively in the present work. The factor $\alpha \exp(-T/\tau_b)$ in the response function associated with the ESA is intended to represent these effects in an ad hoc fashion.

The R_{ge} pathway describes the return of the population from the excited-state e to the ground-state g. If we ignore the nuclear history effect[20] (the imaginary part of $g(t)$), and the rate limiting step is the transition from the dark state to the optically active ground-state g (given by the rate constant $k_{gsr} \sim 1/\tau_c$), we obtain $R_{gg} - R_{ge} \approx R_{gg}^0 \exp(-T/\tau_c)$.

Finally we obtain an approximate expression for the response function

$$R \approx R_{ee}^0 e^{-T/\tau_a} - \alpha \hat{R}_{fe'}^0 e^{-T/\tau_b} + R_{gg}^0 e^{-T/\tau_c} \qquad (10)$$

The first term describes the contribution from the excited-state population when the probe pulse generates a G−E coherence prior to ET (stimulated emission, SE). The second term accounts for a signal arising from the creation of an E−F coherence (i.e. ESA) at any point along the excited-state reaction coordinate (before or after ET). The final term describes the ground-state contribution, which is essentially indicative of solvent fluctuations, but diminishes with the rate of ground-state recovery (GSR). If there was no ET reaction or ESA, then $R = R_{gg}^0 + R_{ee}^0$ (which is the usual expression describing solvation dynamics).

By consideration of this three-level model, we expect to see a rise in the transient absorption and transient grating data if there is an appreciable contribution from the excited-state absorption to the signal, and the reaction coordinate is characterized by large-amplitude nuclear motion (i.e. $\alpha > 0$ and $\tau_b \neq \tau_c$). The peak-shift measurement is sensitive to correlations between the fluctuations on different regions of the potential energy surface (which, in turn, are connected by population kinetics), because it measures the rephasing ability of the system. Thus, the peak-shift decay dynamics depend on the correlation between fluctuations associated with the ground-state absorption transition and those for the excited-state absorption transition. In the case where those fluctuations are perfectly correlated, the signal is scaled by the population dynamics and the peak shift resembles that of the normal two-level system. In contrast, when fluctuations are uncorrelated, the $\hat{R}_{fe'}^0$ contributes a free induction decay (rather than an echo) to the total signal. Then, because of the negative prefactor, a larger peak shift is expected
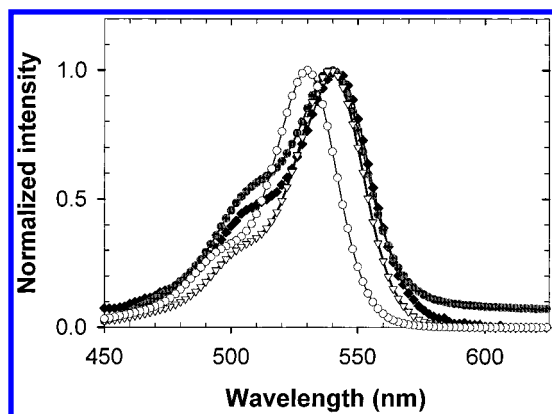
Figure 4. Absorption spectra of R6G in DMA (filled diamonds), DEA (gray circles), DMSO (open triangles), and ethanol (open circles).

at short population times, followed at longer population times by a return to the "normal" level (i.e. consistent with the two-level model) concomitant with repopulation of the ground state (i.e. loss of excited-state population and its associated absorption).

The separation of the response functions from population kinetics in eq 10 (i.e. $R \rightarrow R^0 \exp(-T/\tau_i)$) is based on the work of Onuchic et al.[47,48] They describe a two-coordinate model such that one coordinate represents the solvation dynamics and another coordinate describes the ET reaction coordinate. These workers suggest[47,48] that such a decomposition can be justified by assuming that the signs of the coupling constants between the bath oscillators and the electronic transitions are random and/or that the same bath mode is rarely coupled to both coordinates. In such a case, a separate spectral density may be associated with each coordinate. Moreover, in the present work we observe that the dynamics along the ET coordinate are much faster than those along the solvation coordinate, probably due to the involvement of many intramolecular modes in addition to the high-frequency polarization of the bath. Onuchic et al.[47,48] have shown that in such a case the rate of ET depends only on the ET coordinate.

The experimental observations reported in our work suggest that the fluctuations of the ω_{eg} and ω_{fe} electronic energy gaps are uncorrelated. This can be understood by extending the arguments presented by Onuchic and co-workers[47,48] to four (or more) states, each with different coupling constants to the bath oscillators. Then one expects the fluctuations of ω_{eg}, $\omega_{e'g}$, ω_{fe}, and $\omega_{fe'}$ to be uncorrelated because the signs of the coupling constants are random and/or the same bath mode is rarely simultaneously coupled to all coordinates. In other words, each electronic transition is coupled to a bath of many oscillators that are independent under the assumption of linear response.

IV. Results and Discussion

IV.A. Steady-Sate Spectroscopy. Absorption spectra of rhodamine 6G (R6G) in different solvents are shown in Figure 4. The absorption maximum is blue-shifted in ethanol compared to and DMA and DMSO. The absorption maxima of R6G in DMSO, DMA, and DEA are very similar. We note, however, that the vibronic shoulder is enhanced in DMA and DEA compared to ethanol and DMSO and the spectra of R6G in the electron-donating solvents are slightly broader than in the nonreactive solvents. We attribute this to a larger total coupling strength $\langle \Delta^2 \rangle$ in the reactive solvents as compared to the nonreactive solvents.[49] Vibrational modes that are coupled to the reaction coordinate are likely to have larger displacements

in the reactive solvents and hence larger coupling strengths to the electronic transition.[50,51] Thus, the absorption spectrum will exhibit enhanced vibronic structure and broadening, as we have observed. This is supported by the 3PEPS data reported below, which is a more sensitive probe of line shape. Such an observation highlights the interplay between the solute−solvent interaction and ultrafast dynamics of the excited-state ET reaction.[17] The red side of main absorption band of R6G/DEA has a long tail which may be due to the formation of a charge-transfer complex.

The strong fluorescence emission of R6G in DMSO and ethanol solvents was observed to be almost completely quenched in DMA and DEA solvents. Thus, the excited-state population is removed to a dark state by some process, which we attribute to electron transfer from solvent to solute. The measured lifetime of R6G is approximately 4 ns in various alcohol solvents.[52] Yoshihara et al.[7] reported an excited-state lifetime of less than 6 ps for R6G in DMA (within the instrument response of their picosecond fluorescence up-conversion experiment). In this paper we show that the excited-state lifetime of R6G is ∼85 fs in DMA and ∼160 fs in DEA.

IV.B. Transient Grating Measurements. In transient grating (TG) spectroscopy, two pump pulses create population density in the excited state and a hole in the ground-state population, thus forming a spatial population grating in the sample. The third (probe) pulse is scattered off this grating into the Bragg angle, and its integrated intensity is detected. The grating is destroyed by solvation and population kinetics. For long excited-state lifetimes (e.g. nanoseconds) and in the absence of photoinduced reactions, the TG signal reflects the same solvation dynamics as the peak shift measurement.[38] TG is a homodyne detected method, so the measured signal is the time-integrated modulus squared of the third-order polarization.

Figure 5a shows TG data for R6G in various solvents. It is evident that for nonreactive solvents the signals only decay to ∼30% of the maximum signal within 50 ps. In contrast, the signals for reactive solvents decay almost to zero in 50 ps. Furthermore, the initial decay is much faster in the reactive solvents than nonreactive solvents. We fit the transient grating data with a sum of exponentials for time delays longer than 60 fs (i.e. outside the pulse autocorrelation) to avoid contributions to the signal from nonrephasing diagrams and the ultrafast inertial solvent response.[38] The results are summarized in Table 1. For nonreactive solvents, the time constants obtained from the fits, when multiplied by 2, are in good agreement with the time scales determined from the 3PEPS data, confirming that transient grating and peak-shift measurements reflect the same solvation dynamics. However, for the reactive systems, the excited-state population propagates to a third state after the initial excitation. In addition to the very fast decay and long time slow decay components, we find that a component with negative amplitude (rise) is required to fit the data. This kind of transient rise profile cannot be simply explained as the delay time suggested by models based on diffusion to a sink.[53] Furthermore, the short time-scale component is shorter than that for the nonreactive systems, even though ethanol and DMSO have shorter solvation time scales than DMA and DEA.[54,55] The time scales of the slow decay processes, however, are quite similar to the slower diffusive solvation time scales revealed by the peak-shift measurement as well as those measured by other techniques.[54−56]

Usually population kinetics are convoluted with solvation dynamics; however, by assuming that the solvation contribution to the TG signal for DMA is approximately the same as that
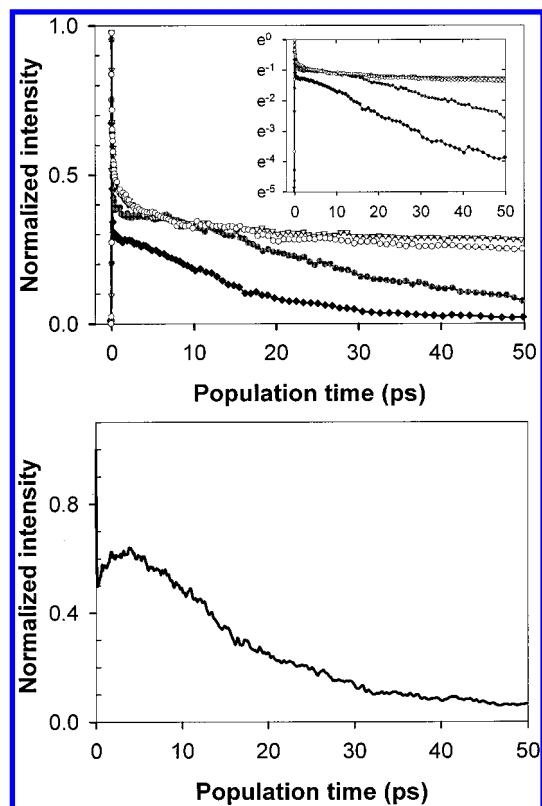
Figure 5. (a, top) Transient grating data for R6G in DMA, DEA, DMSO, and ethanol solvents: (filled diamonds) R6G/DMA, (filled circles) R6G/DEA, (open inverted triangles) R6G/DMSO, and (open circles) R6G/ethanol. (b, bottom): TG signal for R6G/DMA divided by that of R6G/DMSO. A clear rise and decay profile is obtained.

TABLE 1: Fits of Transient Grating Profiles for R6G in Various Solvents[a]

	A_1	$2\tau_1$, fs	A_2	$2\tau_2$, ps	A_3	$2\tau_3$, ps
ethanol	0.51	250	0.20	2.6	0.29	36
DMSO	0.60	265	0.19	3.0	0.20	32
DMA	0.57	150	−0.39	9.7	0.82	21
DEA	0.50	200	−0.67	14.9	1.16	34

[a] Fits begin at $T = 60$ fs. The fitting function is a sum of three exponentials with amplitudes A_i and decay time constants τ_i: $I(T) = \sum_i A_i \exp(-T/\tau_i)$.

for DMSO, we can obtain an approximate separation. Thus, by dividing the transient grating data of R6G in DMA by that for R6G in DMSO, we obtain an approximate picture of the population kinetics (Figure 5b). Here we can see a clear rise and decay, although, to quantify these dynamics, we must turn to a more detailed model.

Quantification requires inclusion of the excited-state absorption contribution to the signal. The excited-state absorption (ESA) of R6G in ethanol has a maximum at 440 nm and submaxima at 400, 530, and 565 nm. The stimulated emission efficiency is observed to be much smaller than expected due to ESA.[57,58] The absorption spectra of R6G/DMA and R6G/DEA in basic solution also show strong structureless absorption in the region between 400 and 580 nm (probably associated with the absorption of the radical R6G•). Hence, to explain the rise in the signal in terms of ESA, we need the three-level model which we described in the previous section (eq 10). To elucidate the reaction kinetics, we need to use that model to simulate the TG data, accounting for both solvation and population dynamics contributions. We first analyze the peak-shift data to obtain the solvation information.
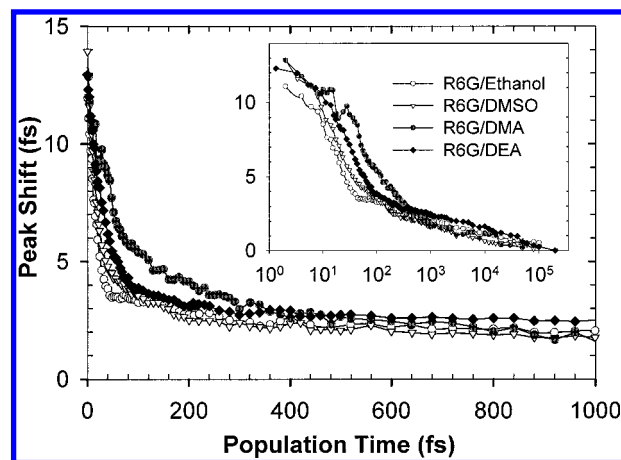

Figure 6. 3PEPS data for R6G in DMA, DEA, DMSO, and ethanol solvents.

TABLE 2: Fits of Peak-Shift Profiles for R6G in Various Solvents[a]

	A_1	τ_1, fs	A_2	τ_2, fs	A_3	τ_3, ps	A_4	τ_4, ps
ethanol	0.75	15	0.12	251	0.07	3.36	0.06	28.1
DMSO	0.62	14	0.22	105	0.11	2.31	0.05	62.0
DMA	0.47	38	0.22	148	0.20	0.57	0.11	20.5
DEA	0.69	31	0.10	225	0.07	3.20	0.14	51.9

[a] The fitting function is a sum of four exponentials with normalized amplitudes A_i and decay time constants τ_i: $\tau(T) = \sum_i A_i \exp(-T/\tau_i)$. At long times only, the fit is approximately proportional to $M(t)$, which enables the τ_3 and τ_4 components to be used as a starting point for the simulations (Table 3).

IV.C. Peak-Shift Measurements. An advantage of the peak shift measurement is that both time scales and amplitudes can provide dynamic information. For example, the initial value of the peak shift is determined largely by the total coupling strength between the electronic transition and the bath (higher total coupling strength leads to a lower initial peak shift), while the asymptotic peak shift is an incisive probe of the long-time inhomogeneity.[23,38]

Figure 6 shows 3PEPS data measured for R6G in ethanol, DMSO, DMA, and DEA. We begin by analyzing the peak shift data using a two-level model in order to retrieve approximate decay time information. For an initial, crude analysis of the data, we simply fit the 3PEPS data with a sum of exponentials. Table 2 summarizes the results of such fits to the peak shift data for R6G in different solvents. At long population times the peak shift follows the transition frequency correlation function $M(t)$, so these fits are useful for obtaining approximately the two picosecond time-scale components arising from diffusive solvent motion (τ_3, τ_4). These components are comparable to the solvation time scales obtained by other workers.[22,54,55] The shortest time scales (τ_1, τ_2) do not correspond directly to the time scales in the underlying correlation function. Simulation is needed to retrieve this short-time information.

Table 3 summarizes the results of such simulations using a pulse duration of 40 fs. Coherently excited vibrational modes are included explicitly in the simulation for nonreactive solvents. For the reactive solvents, we used a Gaussian function as an approximation since the vibrational beats were not well-resolved in those data. The inertial motion was represented by a critically damped Brownian oscillator, with a frequency of $60-80$ cm^{-1}. The diffusive motion was represented by two different exponential contributions to $M(t)$. Two diffusive picosecond time scales were obtained as 1.1 and 26 ps in DMA and 3.2 and 52 ps in DEA. Previous work gave 3.8 and 24.6 ps for DMA and

TABLE 3

(a) Simulations Parameters of Peak-Shift Data for R6G in Various Solvents Based on Two-level System Solvation model

solvents	gaussian[a]		Brownian oscillators[b]			exponentials[c]					
	λ_g cm^{-1}	t_g, fs	λ_b, cm^{-1}	ω_b, cm^{-1}	γ_b, cm^{-1}	λ_1, cm^{-1}	τ_1, ps	λ_2, cm^{-1}	τ_2, ps	λ_3, cm^{-1}	τ_3, ps
DMSO	155	30	120	80	160	100	2.50	20	30	15	200
ethanol	180	30	75	75	150	50	3.55	25	33.6	20	300
DMA	115	40	130	65	130	80	1.10[d]	35	26[d]		
DEA	200	50	120	80	160	42	3.20	85	52		

(b) Vibrational Modes Used in the Simulation of Peak-Shift Data for R6G/DMSO and R6G/Ethanol.[e]

	mode 1	mode 2	mode 3	mode 4
λ, cm^{-1}	60	15	15	10
ω, cm^{-1}	611	402	224	163
τ, fs	50	400	650	500

[a] Additional Gaussian component to compensate for the interference of the unknown modes. For R6G/DMA and DEA only this Gaussian is used. [b] The inertial contribution is modeled as a Brownian oscillator with reorganization energy (λ), frequency (ω), and damping (γ). [c] The exponential contributions are represented by reorganization energy (λ) and decay time (τ). [d] Using an analysis based on the three-level model, we obtain better estimates of these solvation times: $\tau_1 = 3.2$ ps; $\tau_2 = 30$ps. [e] The vibrational modes are represented by damped cosine functions $\exp(-t/\tau_i) \cos(\omega t)$ with reorganization energies λ. All the phases are approximately zero.

TABLE 4: Summary of the Parameters Obtained from the Three-Level Model[a]

solvents	τ_a, fs	τ_b, ps	τ_c, ps	α
DMA	85	4.0	19	0.15
DEA	160	6.9	50	0.20

[a] The τ_i and α are those associated with eq 10.

4.1 and 36.9 ps for DEA, respectively.[54] A detailed analysis of the 3PEPS data requires a three-level model, as examined in section IV.E.

IV.D. Three-Level Model Analysis of the TG Data. To simulate the TG data according to the three-level model, we first obtained good estimates of the SE, ESA, and GSR times of eq 10: τ_a, τ_b, and τ_c by fitting the square root[37,38] of the signal to a sum of exponentials. A more rapid decay of the TG signal is evident during the first 100 fs for the reactive systems compared to the nonreactive systems that we attribute to the ET dynamics. However, this decay is within the coherence period and cannot be resolved directly, so we concentrate on fitting the signal after the first 60 fs. For longer population times, the decay of the signal is dominated by population kinetics, which allowed us to obtain τ_c independently by fitting the tail of the signal. These results are collected in Table 4.

In eq 10, the GSR kinetics are approximated as a single exponential. In fact, we considered the exact kinetic model for the simulations shown in Figure 7. The kinetic time scales were obtained from the fitting of the TG data, and $M(t)$ is determined from the 3PEPS measurement. For DEA, $M(t)$ is taken directly from the two-level model (Table 3) since it is a very similar to the solvation times reported in the literature[54] and the peak shift in DEA is quite similar to that in DMSO and ethanol. However, the peak shift in DMA is distinctly different from the nonreactive solvents, and the time scales of $M(t)$ obtained from the two-level fit are quite different from those reported in the literature.[54] The three-level model is used to obtain a more acurate $M(t)$ for DMA as discussed in section IV.E. We simulated the TG data with and without ESA. We found that introduction of a 15– 20% contribution from ESA significantly improves the fit of the TG data in both DMA and DEA.

According to the three-level model, the three time-scales τ_a, τ_b, and τ_c obtained from this analysis correspond to the stimulated emission lifetime, the excited-state absorption lifetime, and the ground-state recovery time, respectively. We obtain a SE lifetime of 85 and 160 fs for R6G in DMA and DEA,
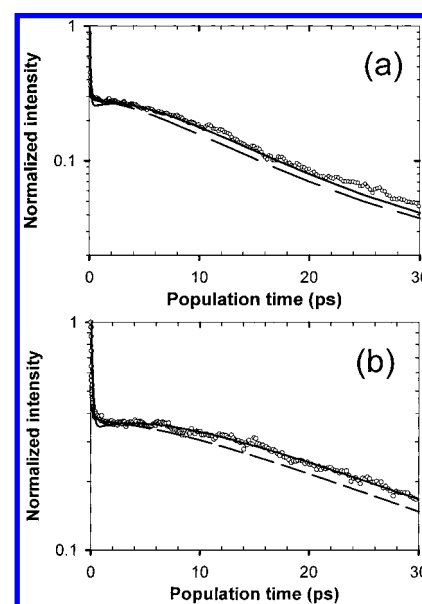

Figure 7. Simulations and experimental data (open circles) for transient grating measurements of (a) R6G/DMA and (b) R6G/DEA. The simulations (solid line) are based on the three-level model with uncorrelated fluctuations between ground-state absorption/stimulated emission and excited-state absorption: 15% ESA for R6G/DMA and 20% R6G/DEA. Simulations without ESA, but including ET (i.e. $\alpha = 0$ in eq 11) are indicated by the dashed line. The simulated curves have been scaled by a factor of ~1.5 in order to assist comparison with the experimental data. This is because we have not accurately simulated the first 60 fs of the signal.

respectively. This is comparable to other work for similar molecules: 80 fs was reported as the electron-transfer rate for oxazine-1/DMA,[8] and 160 fs was reported for nile blue/DMA.[9] We expect the τ_a times obtained from our analysis to provide a reasonable representation of the time scales of electron transfer in R6G/DMA (85 fs) and R6G/DEA (160 fs). Since we fit the data only from 60 fs, the fit provides only an estimate for the actual ET rate, particularly for R6G/DMA. We note that the amplitude of the initial fast decay in the simulation results is slightly larger than in the experimental data. We attribute this to limitations of our model in simulating the first 60 fs of the signal. We assume an incoherent electron-transfer mechanism; that is, the ET does not influence the signal during the coherence period, and the ET kinetics (during the population period) are Markovian. However, the very rapid ET rates we obtained

Ultrafast Photoinduced ET Reactions

J. Phys. Chem. A, Vol. 103, No. 49, 1999 **10355**

suggest that neglect of the reaction during the coherence period may not be a good approximation. Such rapid rates can lead to decay of the population grating even at "zero" population time as a result of the finite pulse duration, giving $R_{ee}(T = 0) < R_{ee}^0$. Such rapid forward ET rates suggest that the reaction is likely to be barrierless and the nuclear reorganization energy is small. In this case the ultrafast inertial solvation dynamics may play a key role in the reaction coordinate and in dissipating excess energy.[17] The charge recombination process, on the other hand, should be an inverted region process due to the energy gap between the charge-separated state and the ground state. In this case the small Franck−Condon factors make the rate commensurately slower.

The ESA lifetimes and GSR times obtained from our simulations are 4.0 and 19 ps for R6G/DMA and 6.9 and 50 ps for R6G/DEA. On the basis of the simple picture described in the previous section, if ESA contributes to the signal for the entire lifetime of the charge-separated state, and the population returns to the ground-state potential surface (G) directly, then τ_b represents the lifetime of the charge-separated state and thus gives an estimate of the back electron transfer rate. The values for τ_b that we have obtained are comparable to the back-electron-transfer rate of 3.8 ps reported for oxazine/DMA by Zinth and co-workers[8] from pump probe measurements. Similarly, Yoshihara and co-workers reported back electron transfer rates of 4.7 ps for oxazine-1/DMA[59] and 4.0 ps for nile blue/DMA[60] by probing the dynamics of the charge-separated state directly.

It is conceivable, however, that the charge-separated state does not return to the original ground state directly, thus introducing a delay time prior to the ground state recovery. For example, the compact ion pair of the charge-separated state may dissociate prior to back-electron transfer and in this process affect the ESA contribution to the signal (e.g. shift it out of resonance with the laser spectrum). Since the product state is expected to be far from equilibrium immediately after formation, it is also possible that relaxation to a precursor state occurs prior to the back-electron transfer.[61,62] In this case, there may be a delay time after the population is removed from the excited state, before the population begins to relax back to ground state. As an alternative, or in addition, the spin-pairing in the e′ state may be changing due to hyperfine couplings.[63−65] It is also possible for such a delay to arise if the hole formed on the DMA (or DEA) donor molecule migrates to another solvent molecule prior to back-ET. Such a process is akin to spatial diffusion of the radical cation and anion molecules away from a compact ion pair geometry, as has been reported previously.[61,62,66−69] The single-wavelength data reported in the present work cannot answer these questions in detail.

If we assume that τ_b gives the approximate time for back electron transfer, then τ_c must define a time scale related to relaxation on the ground-state surface associated with solvation after curve crossing. This is often said to involve "cooling" of the hot ground state. This process involves relxation of both intramolecular and intermolecular (i.e. solvent) modes. The relative amplitude of the two contributions are not obviously a priori, but given the charge separation in the intermediate state and the similarity of the τ_c time with the slowest component in the peak shift data—the diffusive solvation time—we suggest that the τ_c times we report for DMA (19 ps) and DEA (50 ps) correspond to an observation of spectral diffusion on the nonequilibrium ground-state free energy surface. Similarly, a time-scale characteristic of diffusive solvation was observed in fluorescence upconversion studies of the nile blue/DMA system.[60] In the R6G/DMA and R6G/DEA systems the excited-
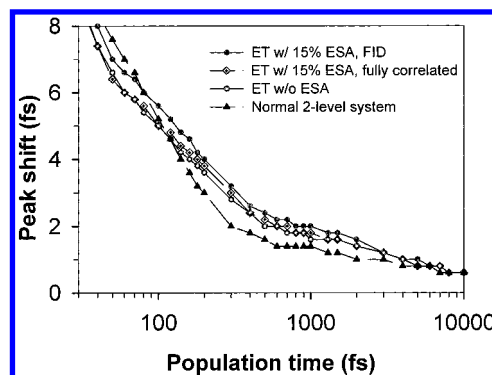

Figure 8. 3PEPS simulations based on four different models: (i) two-level system; (ii) three-state electron transfer without excited state absorption; (iii) three-level electron-transfer model with 15% excited-state contribution (fully correlated fluctuations); and (iv) model iii with uncorrelated fluctuations (leading to free induction decay). In each case the $M(t)$ specified in Table 4 was used together with 40 fs fwhm pulses.

state population undergoes a large Stokes shift by virtue of the electron transfer reaction. Hence, the GSR process involves significant reequilibration of the solvent polarization after back-electron transfer. This process involves dissipation of excess thermal energy, but is rate-limited by the solvation time scales, in close analogy to time-dependent fluoresence measurements of the dynamic Stokes shift in polar solvents.

IV.E. Three-Level Model Analysis of the 3PEPS Data. In a solvated two-level system, the total signal has contributions from ground-state (R_{gg}) and excited-state (R_{ee}) response functions, as well as the interference between the two that derives from the imaginary part of $g(t)$. The imaginary contribution is usually minor at room temperature unless the reorganization energy is particularly large. In a reactive system, the excited-state population and therefore the contribution of R_{ee} is removed by electron transfer to the charge-separated state. Hence, the contributions from the excited-state population and the interference term are lost. This has the effect of increasing the peak shift.[20,70] The higher peak shift observed for R6G in DMA compared to DMSO for population times in the region of 50 fs to hundreds of picoseconds could therefore suggest a smaller contribution from the imaginary part of $g(t)$ owing to the removal of the excited-state population from e−g resonance by the electron-transfer reaction. This is illustrated in the simulations of the 3PEPS data shown in Figure 8. In this figure, the normal two-level system simulation reflects only solvation dynamics. Addition of the ET contribution to the total response function has two effects. First, the peak-shift decays more rapidly at early times (<60 fs) due to the effect of finite pulse duration (as discussed in ref 19), after which it plateaus, thus leading to a higher peak shift over the intermediate time regime than the two-level system.

When the three-level model is used to simulate the 3PEPS data, an imperfect correlation between the nuclear dynamics associated with $\omega_{fe'}$ and ω_{eg} also contributes to the higher peak shift in the intermediate population time region via the ESA contribution to the signal, due to the negative contribution to the response function from the corresponding FID signal. The results of simulations exploring this point for two limiting situations—fully correlated and uncorrelated fluctuations of $\omega_{fe'}$ and ω_{eg}—are also shown in Figure 8. For this small contribution of ESA (15%) to the overall signal, it is difficult to notice significant differences in any of the simulations that include ET. Simulations with larger contributions of the ESA signal showed that models with only ET (i.e. $\alpha = 0$ in eq 10) could not be differentiated from those including ESA if the fluctuations
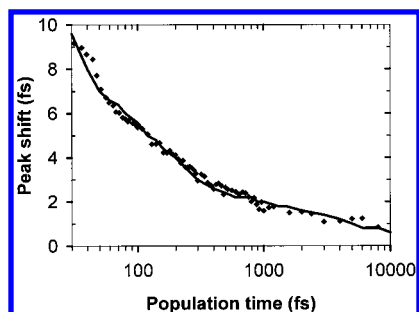
Figure 9. Experimental 3PEPS data for R6G/DMA and the corresponding simulation based on the three-level model. The parameters used are as follows: inertial part is represented by a nearly critically damped Brownian oscillator with coupling strength/frequency/damping of 170 cm^{-1}/60 cm^{-1}/130 cm^{-1} and two exponential components with coupling strength and time scales of 45 cm^{-1}/(3.2 ps) and 20 cm^{-1}/(30 ps). An additional Gaussian component (coupling strength, 65 cm^{-1}; time scale, 30 fs) was used to represent the vibrations.
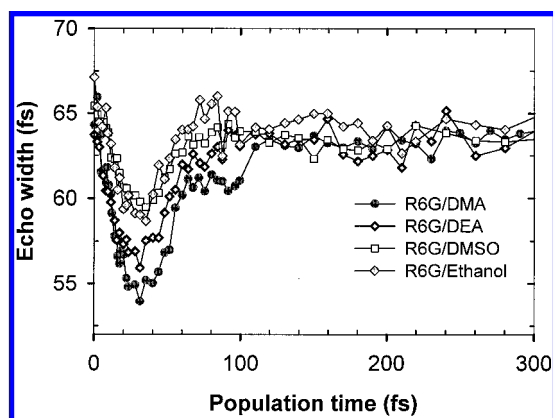

Figure 10. Echo width versus population time of R6G in different solvents: DMA, DEA, DMSO, and ethanol. Note the deeper dip for the reactive solvents compared to the nonreactive solvents.

of the $\omega_{fe'}$ and ω_{eg} energy gaps were fully correlated. However, when the fluctuations were uncorrelated, the negative FID contribution to the response function increased the peak shift for the intermediate time scales. In Figure 9 we compare a simulation based on the three-level model with a 15% FID ESA contribution (i.e. $\alpha = 0.15$ in eq 10) with the peak shift data for R6G/DMA. The two solvation time scales obtained are 3.2 and 30 ps, which are now similar to those reported for DMA (3.8 and 24.6 ps),[54] in contrast to those obtained from analysis of the data using a two-level model. The kinetic parameters used in these simulations were obtained from analysis of the TG data, as described in section IV.D.

IV.F. Coupling of Electron Transfer to High-Frequency Vibrations. It is possible that the extremely fast ET couples to high-frequency vibrational motion.[29,71,72] Zinth et al.[8] reported that ET dynamics in the oxazine/DMA system are modulated by an aromatic ring breathing mode of ca. 600 cm^{-1} (55 fs period). A strong 611 cm^{-1} mode has been observed in a resonance Raman study of R6G in methanol.[73] We might expect to see indications of this as differences in the coherently excited vibrational wave packets in the peak-shift data for the reactive system compared to the nonreactive systems. Inspection of the R6G/DMA peak-shift data (Figure 6) reveals oscillations at early times, which correlate with a strong quantum beat in a plot of echo width versus population period. This dynamic narrowing of the width of the echo signal is seen clearly as the dip in the plot of echo fwhm versus population time, Figure 10. This dip appears at the same population time for both reactive and nonreactive systems, suggesting that it is modulated by the same

vibrational frequency in all cases studied. The minimum of the dip position is 59 fs for R6G in both DMSO and ethanol solvents. However, the amplitude of this dip is markedly larger in the reactive systems than in the nonreactive systems with the minimum being at 53 fs in DMA and 56 fs in DEA, respectively. This suggests that the coupling of the electronic transition to this vibration is larger in the reactive solvents than the nonreactive solvents. Intramolecular reorganization along the reaction coordinate may thus involve this mode, which is in accord with the different vibronic intensity of the corresponding band in the absorption spectra for the reactive solvents versus the nonreactive solvents (Figure 4).

V. Conclusions

Transient grating (TG) and three-pulse photon echo peak shift (3PEPS) measurements were used to investigate ultrafast electron transfer in R6G/DMA and R6G/DEA electron-donating solvent systems. A purpose of the present investigation was to ask whether 3PEPS probes aspects of reaction dynamics that would otherwise be obscured by population dynamics or lack of sufficient time resolution. New methods were employed in order to model these data using nonlinear response functions expressed in terms of both solvation dynamics and reaction kinetics.

There are three distinct dynamical contributions to the signals reported here: stimulated emission, excited-state absorption, and ground-state recovery. We have found that by modeling the dynamics of ultrafast electron transfer from solvent to solute in the R6G/DMA and R6G/DEA systems using nonlinear response functions derived from the three-level model, Figure 3, we could obtain a large dynamic range of kinetic information in addition to the details of solvation dynamics. Even though the initially generated excited state decayed rapidly (via ET) to a product that gave no stimulated emission signal at our excitation wavelength, and therefore contributed no excited-state response function in the usual manner, we were able to monitor the reaction in the product region of the surface via excited-state absorption. This enabled us to retrieve kinetic information over a larger range of time scales than would otherwise be possible with a one-color measurement. Similarly, Bagchi et al.[45] concluded for barrierless reactions that fluorescence studies measure population decay from a small part of the excited-state surface and are sensitive to population relaxation on this surface, while GSR and ESA provide information on the population sink between excited state and ground state. Furthermore, by combining the TG and 3PEPS methods, we also obtained detailed information on the solvation dynamics and their entanglement with the ET reaction.

Two coordinates are often associated with electron-transfer reactions. One corresponds primarily to intramolecular configurational and frequency changes between the reactant and product states, where as the other corresponds to the solvation coordinate. The analysis reported in the present work using the three-level model suggests that the solvation process and the ET reaction can be considered to be essentially independent of each other in this system, despite the rapid kinetics of the reaction.

The rate of ET is much faster than the rate of back-ET in the systems we are studying, which means that the macroscopic grating in the sample is preserved even after ET. Thus, we observed a signal from the gg pathway until such a time as the hole in the ground-state population density was destroyed by back electron transfer and cooling. We modeled this as $R_{gg} - R_{ge} \approx R_{gg}^0 \exp(-T/\tau_c)$. Thus, the rate of GSR is defined by τ_c.
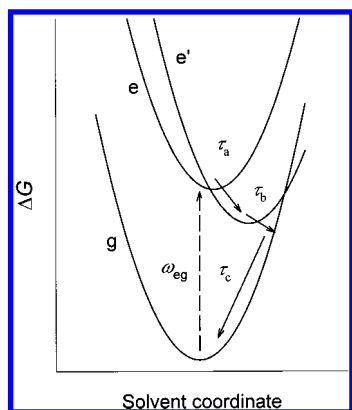
Figure 11. Model free energy curves that summarize our conclusions drawn from analysis of the R6G/DMA data based on the three-level model, eq 10.

Stimulated photon echoes in systems where such optical branching occurs have been reported previously by Wiersma and co-workers.[74] Consideration of the similarity of this time scale to that for solvation in both DMA and DEA solvents led us to conclude that the rate of GSR is determined by spectral diffusion on the ground-state free energy surface, as depicted in Figure 11.

Understanding the signal arising from the excited-state population was more complicated because of the ET dynamics and ESA contributions to the response function. In the simplest situation the ET reaction is incoherent (Markovian) and has the effect of depleting the ee population according to the rate of ET: $R_{ee}^0 \exp(-T/\tau_a)$. In addition, in the present work we found good evidence that we can probe the product region of the excited-state surface, e′e′, via ESA. The complex evolution of this contribution to the signal was modeled in a simple fashion via $-\alpha \hat{R}_{fe'} \exp(-T/\tau_b)$. We suggest that τ_b is a good indication of the back electron transfer rate.

We conclude that, for R6G/DMA, rapid photoinduced ET occurs on a time scale of $\tau_a \sim 85$ fs and for the R6G/DEA system $\tau_a \sim 160$ fs. An excited-state absorption contribution to the signals characterized by time scale $\tau_b = 4.0$ ps for R6G/DMA (15% contribution) and $\tau_b = 6.9$ ps for R6G/DEA (20% contribution) was associated with back-electron transfer. Subsequently, the cooling and relaxation (i.e. ground-state recovery) occurs on time scales of $\tau_c = 19$ ps (R6G/DMA) and $\tau_c = 50$ ps (R6G/DEA), which we attribute to solvent-limited reequilibration on the ground-state free energy curve after back-electron transfer.

References and Notes

(1) Marcus, R. A. *J. Chem. Phys.* **1956**, *24*, 996.
(2) Marcus, R. A. *Annu. Rev. Phys. Chem.* **1964**, *15*, 155.
(3) Marcus, R. A.; Sutin, N. *Biochim. Biophys. Acta* **1985**, *811*, 155.
(4) Sumi, H.; Marcus, R. A. *J. Chem. Phys.* **1986**, *87*, 4894.
(5) Maroncelli, M.; MacInnis, J.; Fleming, G. R. *Science* **1989**, *243*, 1674.
(6) Andrews, D. P.; McFadyen, G. G.; Beddard, G. S. *Chem. Phys. Lett.* **1998**, *293*, 343.
(7) Kemnitz, K.; Yoshihara, K. *Chem. Lett.* **1991**, 645.
(8) Seel, M.; Engleitner, S.; Zinth, W. *Chem. Phys. Lett.* **1997**, *275*, 363.
(9) Yoshihara, K.; Nagasawa, Y.; Yartsev, A.; Johnson, A. E.; Tominaga, K. *J. Mol. Liq.* **1995**, *65−6*, 59.
(10) Kuznetsov, A. M. *Charge transfer in physics, chemistry and biology: physical mechanisms of elementary processes and an introduction to the theory*; Gordon and Breach Publishers: Amsterdam, New York, 1995.
(11) Bendall, D. S. *Protein electron transfer*; Bios Scientific: Oxford, U.K., 1996.
(12) Breton, J.; Vermeglio, A. *The Photosynthetic Bacterial Reaction Center II: Structure, Spectroscopy, and Dynamics*; Plenum Press: New York, 1992.
(13) Hush, N. S. *Electrochim. Acta* **1968**, *13*, 1005.
(14) Newton, M. D.; Sutin, N. *Anuu. Rev. Phys. Chem* **1984**, *35*, 437.
(15) Okada, A.; Chernyak, V.; Mukamel, S. *J. Phys. Chem. A* **1998**, *102*, 1241.
(16) Jortner, J.; Bixon, M.; Ratner, M. A. *Proc. Indian Acad. Sci.* **1997**, *109*, 365.
(17) Bagchi, B.; Gayathri, N. *Adv. Chem. Phys.* **1999**, *107*, 1.
(18) Kosower, E. M.; Huppert, D. *Annu. Rev. Phys. Chem.* **1986**, *37*, 127.
(19) Zusman, L. D. *Chem. Phys.* **1980**, *49*, 295.
(20) Yang, M.; Ohta, K.; Fleming, G. R. *J. Chem. Phys.* **1999**, *110*, 10243.
(21) Ladanyi, B. M.; Stratt, R. M. *J. Phys. Chem.* **1995**, *99*, 2502.
(22) Passino, S. A.; Nagasawa, Y.; Joo, T.; Fleming, G. R. *J. Phys. Chem. A* **1997**, *101*, 725.
(23) Fleming, G. R.; Cho, M. *Annu. Rev. Phys. Chem.* **1996**, *47*, 109.
(24) Rips, I.; Jortner, J. *J. Chem. Phys.* **1987**, *87*, 6513.
(25) Rips, I.; Jortner, J. *J. Chem. Phys.* **1988**, *88*, 818.
(26) Rips, I.; Klafter, J.; Jortner, J. *J. Phys. Chem.* **1990**, *94*, 8557.
(27) Rosenthal, S. J.; Xie, X.; Du, M.; Fleming, G. R. *J. Chem. Phys.* **1991**, *95*, 4715.
(28) Chandra, A.; Bagchi, B. *Chem. Phys.* **1991**, *156*, 323.
(29) Yoshihara, K.; Tominaga, K.; Nagasawa, Y. *Bull. Chem. Phys. Jpn.* **1995**, *68*, 696.
(30) Schneider, S.; Stammler, W.; Bierl, R.; Jager, W. *Chem. Phys. Lett.* **1994**, *219*, 433.
(31) Shannon, C. F.; Eads, D. D. *J. Chem. Phys.* **1995**, *103*, 5208.
(32) Wolfseder, B.; Seidner, L.; Domcke, W.; Stock, G.; Seel, M.; Engleitner, S.; Zinth, W. *Chem. Phys.* **1998**, *233*, 323.
(33) Wynne, K.; Galli, C.; Hochstrasser, R. M. *J. Chem. Phys.* **1994**, *100*, 4797.
(34) Cho, M.; Hu, Y.; Rosenthal, S. J.; Todd, D. C.; Du, M.; Fleming, G. R. Friction Effects and Barrier Crossing. In *Activated Barrier Crossing, Applications in Physics, Chemistry and Biology*; Fleming, G. R., Hanggi, P., Eds.; World Scientific: London, 1993; p 143.
(35) Åberg, U.; Åkesson, E.; Fedchenia, I.; Sundström, V. *Isr. J. Chem.* **1993**, *33*, 167.
(36) Joo, T. H.; Jia, Y. W.; Yu, J. Y.; Jonas, D. M.; Fleming, G. R. *J. Phys. Chem.* **1996**, *100*, 2399.
(37) Mukamel, S. *Principles of nonlinear optical spectroscopy*; Oxford University Press: New York, 1995.
(38) Joo, T. H.; Jia, Y. W.; Yu, J. Y.; Lang, M. J.; Fleming, G. R. *J. Chem. Phys.* **1996**, *104*, 6089.
(39) Cho, M. H.; Yu, J. Y.; Joo, T. H.; Nagasawa, Y.; Passino, S. A.; Fleming, G. R. *J. Phys. Chem.* **1996**, *100*, 11944.
(40) de Boeij, W. P.; Pshenichnikov, M. S.; Wiersma, D. A. *J. Phys. Chem.* **1996**, *100*, 11806.
(41) Breton, J.; Martin, J.-L.; Fleming, G. R.; Lambry, J.-C. *Biochemistry* **1988**, *27*, 8276.
(42) Rettig, W. *Top. Curr. Chem.* **1994**, *169*, 254.
(43) Lippert, E.; Rettig, W. *Adv. Chem. Phys.* **1987**, *68*, 1.
(44) Vogel, M.; Rettig, W. *Chem. Phys. Lett.* **1988**, *147*, 452.
(45) Bagchi, B.; Åberg, U.; Sundström, V. *Chem. Phys. Lett.* **1989**, *162*, 227.
(46) Ben-Amotz, D.; Harris, C. B. *Chem. Phys. Lett.* **1985**, *119*, 305.
(47) Onuchic, J. N.; Beraton, D. N.; Hopfield, J. J. *J. Phys. Chem.* **1986**, *90*, 3707.
(48) Onuchic, J. N. *J. Chem. Phys.* **1987**, *86*, 3925.
(49) Marcus, R. A. *J. Chem. Phys.* **1965**, *43*, 1261.
(50) Markel, F.; Ferris, N. S.; Gould, I. R.; Myers, A. B. *J. Am. Chem. Soc.* **1992**, *114*, 6208.
(51) Scholes, G. D.; Fournier, T.; Parker, A. W.; Phillips, D. *J. Chem. Phys.*, in press.
(52) Gumy, J. C.; Vauthey, E. *J. Phys. Chem.* **1996**, *100*, 8628.
(53) Bagchi, B.; Fleming, G. R.; Oxtoby, D. W. *J. Chem. Phys.* **1983**, *78*, 7375.
(54) Shirota, H.; Pal, H.; Tominaga, K.; Yoshihara, K. *J. Phys. Chem. A* **1998**, *102*, 3089.
(55) Horng, M. L.; Gardecki, J. A.; Papazyan, A.; Maroncelli, M. *J. Phys. Chem.* **1995**, *99*, 17311.
(56) Smith, N. A.; Lin, S. J.; Meech, S. R.; Shirota, H.; Yoshihara, K. *J. Phys. Chem. A* **1997**, *101*, 9578.
(57) Magde, D.; Gaffney, S. T.; Campbell, B. F. *IEEE J. Quantum Electron.* **1981**, *QE−17*, 489.

(58) Sahar, E.; Treves, D. *IEEE J. Quantum Electron.* **1977**, *QE−13*, 962.

(59) Yoshihara, K.; Nagasawa, Y.; Yartsev, A.; Kumazaki, S.; Kandori, H.; Johnson, A. E.; Tominaga, K. *J. Photochem. Photobiol., A* **1994**, *80*, 169.

(60) Kandori, H.; Kemnitz, K.; Yoshihara, K. *J. Phys. Chem.* **1992**, *96*, 8042.

(61) Gould, I. R.; Young, R. H.; Moody, R. E.; Farid, S. *J. Phys. Chem.* **1991**, *95*, 2068.

(62) Asahi, T.; Mataga, N. *J. Phys. Chem.* **1989**, *93*, 6575.

(63) Werner, U.; Staerk, H. *J. Phys. Chem.* **1995**, *99*, 248.

(64) Vogelmenn, E.; Kramer, H. *Photochem. Photobiol.* **1976**, *24*, 595.

(65) Iwa, P.; Steiner, U. E.; Vogelmann, E.; Kramer, H. *J. Phys. Chem.* **1982**, *86*, 1277.

(66) Vauthey, E.; Parker, A. W.; Nohova, B.; Phillips, D. *J. Am. Chem. Soc.* **1994**, *116*, 9182.

(67) Knibbe, H.; Rollig, K.; Schafer, F. P.; Weller, A. *J. Chem. Phys.* **1967**, *47*, 1184.

(68) Taniguchi, Y.; Nishina, Y.; Mataga, N. *Bull. Chem. Soc. Jpn.* **1972**, *45*, 764.

(69) Vauthey, E.; Hogemann, C.; Allonas, X. *J. Phys. Chem. A* **1998**, *102*, 7362.

(70) Nagasawa, Y.; Passino, S. A.; Joo, T.; Fleming, G. R. *J. Chem. Phys.* **1997**, *106*, 4840.

(71) Barbara, P. F.; Walker, G. C.; Smith, T. P. *Science* **1992**, *256*, 975.

(72) Walker, G. C.; Ckesson, E.; Johnson, A. E.; Levinger, N. E.; Barbara, P. F. *J. Phys. Chem.* **1992**, *96*, 3728.

(73) Kwok, A. S.; Chang, R. K. *Opt. Lett.* **1993**, *18*, 1703.

(74) Morsink, J. B. W.; Wiersma, D. A. *Chem. Phys. Lett.* **1979**, *65*, 105.